Experimental and Theoretical Study of Triplet Energy Transfer in Rigid Polymer Films

Paul B. Merkel* and Joseph P. Dinnocenzo*

Department of Chemistry and the Center for Photoinduced Charge Transfer, University of Rochester, Rochester, New York 14627-0216

Received: March 12, 2008; Revised Manuscript Received: August 18, 2008

With the judicious selection of triplet energy donor (D) and acceptor (A) pairs, a laser flash photolysis procedure has provided a sensitive method for the study of triplet energy transfer in rigid polymer films. By monitoring changes in triplet−triplet (T−T) absorptions the kinetics of triplet energy transfer were evaluated at short time scales, and overall energy-transfer quantum yields were also obtained. Combinations of xanthone- or thioxanthone-type donors and polyphenyl acceptors were particularly suited to these measurements because the former have high intersystem-crossing quantum yields and the latter have very high extinction coefficients for T−T absorption. For exothermic transfer most of the energy transfer that occurred within the lifetime of triplet D (^{3}D) took place in less than a few microseconds after ^{3}D formation in poly(methyl methacrylate), and triplet A yields were limited largely by the number of A molecules in near contact with ^{3}D. The kinetics of triplet energy transfer were modeled using a modified Perrin-type statistical arrangement of D/A separations with allowance for excluded volume in combination with a Dexter-type formula for the distance-dependent exchange energy-transfer rate constant. Experimental observations were best explained by constraining D/A separations to reflect the dimensions of intervening molecules of the medium. Rate constants, k_0, for exothermic energy transfer from ^{3}D to A molecules in physical contact are approximately 10^{11} s^{-1} and very similar to triplet energy-transfer rate constants determined from solution encounters. Energy-transfer rate constants, $k(r)$, fall off as approximately $\exp(-2r/0.85)$, where r is the separation distance between D and A centers in angstroms. Exchange energy transfer is not restricted to ^{3}D and A in physical contact, but at $\leq$0.4 M A at least 85% of the energy transfer arises from interaction of ^{3}D with a single nearest-neighbor A molecule. The modified Perrin model was also applied to quantum yields of quenching in rigid media. Comparison to the simple Perrin model for quenching shows that the latter may be adequate as long as molecular volumes are accommodated in the Perrin expression. Under these conditions the critical radius, r_c, corresponds to the ^{3}D/A separation at which the effective rate constant for energy transfer equals the inverse of the ^{3}D lifetime.

1. Introduction

Energy transfer from a triplet energy donor (D) or sensitizer to a triplet energy acceptor (A) is an important step in many photochemical processes, including processes in polymers and other rigid media. Triplet energy transfer can play a role in photosynthesis[1] and energy upconversion[2] and has been of particular recent interest in electrophosphorescent materials, including organic light-emitting diode (OLED) devices[3] and polymeric light-emitting diode (PLED) devices.[4] In addition, efficient polymeric information storage media that utilize triplet energy transfer have recently been described.[5] Furthermore, triplet energy transfer is conceptually related to electron transfer,[6] which is also involved in many photophysical and photochemical processes, including solar energy conversion.[7−9]

The kinetics of the short-range process of triplet energy transfer via electron exchange in rigid or high-viscosity media has not been fully characterized, particularly at short times. Prior studies of triplet energy transfer in rigid media have focused primarily on steady-state or pulsed measurements of phosphorescence quenching,[3c,10−18] including some measurements in the microseconds time regime[3c,12,13,18] and in polymer films.[3c,16−18] The conceptually similar process of rapid electron transfer in rigid media has been extensively studied experimentally and theoretically.[19] There have also been limited studies of triplet energy transfer in rigid media utilizing triplet−triplet absorption measurements.[4,20,21] The experimental method described herein utilized laser flash photolysis to monitor the decay of triplet D (^{3}D) and buildup of triplet A (^{3}A) in rigid polymer films, such as poly(methyl methacrylate) (PMMA). The buildup of ^{3}A has provided a particularly sensitive method for probing the kinetics and efficiency of triplet energy transfer with proper choice of A. Polyphenyl derivatives such as *p*-terphenyl (PTP) were particularly suitable as A due to their high extinction coefficients ($\sim 10^5$ M^{-1} cm^{-1}) for triplet−triplet (T−T) absorption.[22a] Xanthone and thioxanthone derivatives were particularly suitable as D due to their high extinction coefficients, very high intersystem-crossing quantum yields ($\sim$0.99) and rate constants ($\sim 10^{11}$ s^{-1}),[22] and location of their T−T absorptions in a different spectral region ($\sim$650 nm) than the polyphenyls ($\sim$420−470 nm).[22a] The experimental kinetic and efficiency data obtained by laser photolysis of polymer films containing D and A have been analyzed in terms a combination of a statistical, Perrin-type[23] distribution of D/A separations and a Dexter-type[24] distant-dependent rate constant for exchange energy transfer. While similar analyses have been utilized previously to fit the decay of donor phosphorescence[11−16,20] or electron transfer[19] in rigid media, modification was required for application to the buildup of ^{3}A, which is particularly informative in short time regimes. A proper analysis also required inclusion of the effects of the excluded volumes of D and A on statistical distributions. As will be described, the analysis has provided values for the

* To whom correspondence should be addressed. E-mail: pmerkel@rochester.rr.com; jpd@chem.rochester.edu.

10.1021/jp802164d CCC: $40.75
Published on Web 10/04/2008

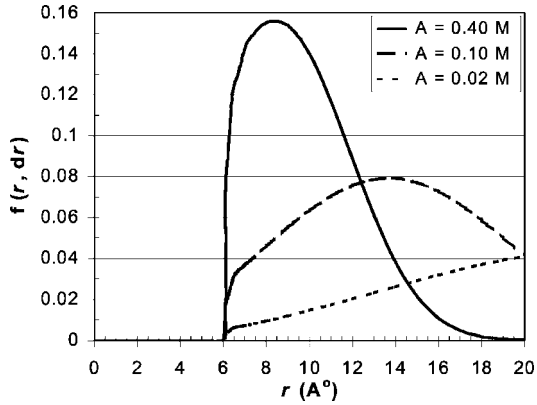

Figure 1. Fractions, f(r,dr), of ^{3}D molecules with nearest-neighbor A molecules centered in 1 Å spherical shells at D/A separation distances of r (Å) for 0.02, 0.10, and 0.40 M A with $r_0 = 6$ Å and $r_A = 3$ Å.

rate constant, k_0, for energy transfer from D to A molecules in physical contact and the characteristic parameter, L, for the exponential fall off in the energy-transfer rate constant.

The experimental methods utilized here for evaluation of T−T energy transfer have several advantages. Use of pulsed laser excitation allowed analysis at short times during which most of the energy transfer typically takes place. Measurements in polymer films could be carried out at ambient temperature and with high D and A concentrations relevant to practical materials. Finally, use of A with high extinction coefficients for T−T absorption enhanced sensitivity and allowed lower pulse energies to minimize photodegradation and decay via T−T annihilation.

2. Experimental Section

2.1. Materials. Poly(methyl methacrylate) with a molecular weight of about 25 000 (Polysciences, Inc.) was used in these experiments. The donor 2-*t*ert-pentylxanthone (PXAN) and acceptor dibutyl-3,3′-terphenyldicarboxylate (TPDC) were provided by D. Robello of Eastman Kodak Co. and prepared and purified as previously described.[5] The commercially available donor 2,4-diethyl-thioxanthone (DETX) and acceptors *p*-terphenyl (PTP) and dimethyl-4,4′-biphenyldicarboxylate (BPDC) were purified by recrystallization. The acceptors PTP, BPDC, and TPDC have extinction coefficients for T−T absorption in ethyl acetate of 81 000 (at 445 nm), 85 000 (at 419 nm), and 82 000 M^{-1} cm^{-1} (at 451 nm), respectively,[22a] which facilitated measurement of triplet concentrations. Poly(ethylene terephthalate) film support was provided by Eastman Kodak Co.

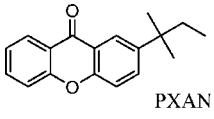

PXAN

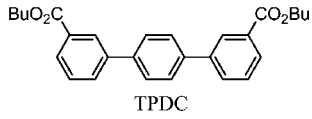

TPDC

2.2. Film Preparation. PMMA films containing D and A were prepared by coating them onto transparent poly(ethylene terephthalate) support with a thin adhesion layer, such as 0.5 μm of poly(acrylonitrile-co-vinylidene chloride-co-acrylic acid) (14:80:6). A typical coating solution consisted of about 10 mg of D, about 10−200 mg of A, and 1.00 g of PMMA dissolved in 4.0 mL of warmed dichloromethane solvent. The solutions were applied with a 5 mil (127 μm) coating knife onto a support held by vacuum on a metal coating block at 25 °C. After air drying for 10 min, the films were further dried in a vacuum oven at 40 °C for 4 h. Final film thickness was about 25 μm.

2.3. Laser Flash Photolysis Measurements. Triplet−triplet absorption spectra and triplet formation and decay kinetics were measured using a nanosecond laser flash photolysis apparatus. A Lambda Physik Lextra 50 XeCl excimer laser was used to pump a Lambda Physik 3002 dye laser, providing approximately 7 ns pulses with an energy of about 2 mJ. Measurements were carried out using either 343 nm excitation (with *p*-terphenyl as the laser dye) or 400 nm excitation (with diphenylstilbene). Transient absorptions were monitored at 90° to the laser excitation using pulsed xenon lamps, timing shutters, a monochromator, and a photomultiplier tube for kinetic measurements or a diode array detector for obtaining transient absorption spectra. For kinetic analyses the signal from the photomultiplier tube was directed into a Tektronix TDS 620 digitizing oscilloscope and then to a computer for viewing, storage, and analysis. Typically, beam energies were attenuated to less than 1 mJ per pulse to minimize photochemical reaction products and T−T annihilation, and data were averaged over at least 20 pulses. Film samples were orientated at 45° to the laser light, such that surface reflections were directed toward the analyzing lamp rather than the photodetector. For measurements under argon, films were placed in 1 cm quartz cells fitted with a rubber cap pierced by two syringe needles to provide for argon inflow and outflow.

3. Kinetic Models

3.1. Perrin Model and Differential Distribution Expression. The models used to analyze experimental kinetic and efficiency data for triplet energy transfer in rigid media consisted essentially of determining the distributions of separation distances, r, between various D and A molecules and the distant-dependent rate constants for energy transfer, $k(r)$, and then summing all A contributions, $\Sigma k(r)$, to the quenching of ^{3}D molecules. A simpler version of this model was introduced by Perrin[23] and is often still used to analyze quenching by electron exchange and electron transfer in rigid media. This model assumes that there is a quenching sphere of radius r_c about an excited molecule within which quencher molecules deactivate with unit efficiency and outside of which no quenching occurs. In the Perrin model the amount of quenching of ^{3}D molecules by A is determined by the concentration-dependent statistical distribution of A molecules around D, which is readily calculated by probability theory. The fraction F(r_c) of ^{3}D with at least one molecule of A within r_c or equivalently the fraction of ^{3}D quenched is given in terms of the molar concentration of A and with r_c expressed in angstroms by eq 1

$$F(r_c) = 1 - \exp(-0.00252 r_c^3[A]) \quad (1)$$

The probability considerations that lead to eq 1 are based on the volume of a sphere of radius r_c relative to the total volume available to A molecules assuming that D and A are point particles. More realistically, if D and A are considered to have effective radii, r_D and r_A, respectively, then within the sphere of radius r_c the available volume is reduced by the contact or encounter volume of a sphere of radius $r_0 = r_D + r_A$. Correcting for the excluded contact volume[18] eq 1 becomes eq 2

$$F(r_c) = 1 - \exp\{-0.00252(r_c^3 - r_0^3)[A]\} \quad (2)$$

The effect of excluded contact volume can become significant for short-range quenching processes such as electron exchange.

A more accurate treatment also recognizes the fact that D and A may occupy a significant fraction of the total volume.[25] The effect of typical low concentrations of D on the available total volume can usually be neglected. However, at high A

concentrations the volume occupied by A molecules should be included in probability considerations. As molecules of A are added, the total unoccupied volume available to the next A molecule is reduced by the total contact volume of previously added A molecules. On average the available total volume is reduced by one-half of the total contact volume of A molecules associated with a given A concentration. The fractional excluded total volume is therefore given by $V_{ex} = 0.5(0.00252)(2r_A)^3[A]$, where $2r_A$ is the radius of the encounter sphere for two A molecules. This can be used to determine an effective A concentration, given by eq 3, that may be used in eq 2

$$[A]' = [A]/(1 - 0.0101r_A^3[A]) \quad (3)$$

The Perrin model can be further refined by assigning a particular rate constant, $k(r)$, to each r and using the distribution of nearest-neighbor separation distances. The fraction, $f(r,dr)$, of ^3D molecules having nearest-neighbor A molecules centered within a thin shell of thickness dr at a distance r can be obtained simply by replacing r_c by r in eq 2 and differentiating to obtain eq 4

$$dF(r) \text{ or } f(r,dr) = 0.00756r^2[A]' \exp\{-0.00252(r^3 - r_0^3)[A]'\}dr \quad (4)$$

with r and r_0 in angstroms and $[A]'$ given by eq 3. The distribution function, $f(r,dr)$, is plotted vs r in Figure 1 for acceptor concentrations of 0.02, 0.10, and 0.40 M with $r_0 = 6$ Å, $r_A = 3$ Å, and $dr = 1$ Å. The plots in Figure 1 show the fractions of ^3D molecules having nearest-neighbor A molecules with centers in 1 Å thick spherical shells at various separation distances allowing for excluded contact volume and excluded total volume. The sums of the fractions for successive 1 Å thick shells beginning at 6.5 Å or equivalently the areas under the curves in Figure 1 taken to large r are all unity. Equation 4 is equivalent to the nearest-neighbor distribution law previously derived by a slightly different method.[26] We will subsequently show that quenching by nearest neighbors dominates energy transfer but will also explicitly include in our model the typically small effects of quenching by A molecules in shells further removed than the nearest-neighbor shell. We will also include the effects of multiple A occupancy in some nearest-neighbor shells in accordance with probability theory.

3.2. Dexter Expression. According to an analysis by Dexter[24] the rate constant for the transfer of triplet energy via electron exchange varies exponentially with the D/A separation distance, r, according to eq 5

$$k(r) = A \exp(-2r/L) \quad (5)$$

where A is a frequency factor and L is the effective average Bohr radius of the interacting orbitals. For nonspherical molecules or molecules with excitations involving nonspherical electronic orbitals a simple exponential falloff of $k(r)$ represents an approximation[19d,27] that can at least serve as a reasonable starting point. Long-range processes such as dipole−dipole (resonance) energy transfer are relatively unimportant for triplet energy transfer. Thus, the rapid falloff in exchange energy transfer expressed by eq 5 requires that D and A be in near contact for energy transfer to compete with other decay processes.

At r_0, the sum of the effective van der Waals radii of D and A, $k(r)$ may be referred to as k_0 and expressed by eq 6

$$k_0 = A \exp(-2r_0/L) \quad (6)$$

Solving eq 6 for A and substituting into eq 5 allows the Dexter expression to be rewritten as eq 7

SCHEME 1

$$^3D + A \underset{k_{-d}}{\overset{k_d}{\rightleftharpoons}} (^3D \cdots A) \underset{k_{-et}}{\overset{k_{et}}{\rightleftharpoons}} (D \cdots {}^3A) \xrightarrow{k_{-d}} D + {}^3A$$

$$k(r) = k_0 \exp[-2(r - r_0)/L] \quad (7)$$

Suitable values for r_0 can be determined from calculated van der Waals volumes, v_D and v_A, of D and A, respectively. For the molecules used in our experiments the calculated[28] v_D and v_A values are approximately 250−300 Å^3. For a parallel close-approach orientation of the somewhat planar D and A molecules of our studies $r_0 \approx [3(v_D + v_A)/4\pi]^{1/3}$ or ∼5 Å, whereas for spherical molecules $r_0 = (r_D + r_A)$ or ∼8 Å. We used an r_0 of 6 Å as a compromise.

A starting estimate for k_0 for use in eq 7 may be obtained from solution energy-transfer experiments as described below. Bimolecular processes in solution are commonly analyzed via the encounter complex model, which for triplet energy transfer is represented by Scheme 1, where k_d is the rate constant for diffusional formation of the encounter complex, k_{-d} is the rate constant for separation of the encounter pair, and k_{et} and k_{-et} are the respective rate constants for forward and reverse energy transfer within the encounter complex.

When energy transfer is suitably exothermic (≥2 kcal/mol), k_{-et} is small relative to k_{-d} and the experimental energy-transfer rate constant, k_{en}, is given by eq 8

$$k_{en} = k_d k_{et}/(k_{-d} + k_{et}) \quad (8)$$

which rearranges to eq 9

$$k_{et} = k_{en} \times k_{-d}(k_d - k_{en}) \quad (9)$$

The encounter complex may be considered to consist of repeated collisions within a solvent cage having a radius of nominally ∼1 Å greater than r_0. This allows estimation of k_0 from eq 7 and k_{et}, which may be calculated from k_{en}, k_d, and k_{-d} according to eq 9. In solutions of low viscosity (∼0.5 cp), k_{en} values for moderately exothermic triplet energy transfer are often about $6-8 \times 10^9$ M^{-1} s^{-1}.[29] For example, we measured $k_{en} = 7 \times 10^9$ M^{-1} s^{-1} for the quenching of triplet PXAN ($E_T = 71.3$ kcal/mol)[22a] by TPDC ($E_T = 60.6$ kcal/mol)[22a] in ethyl acetate.

A reasonable estimate for k_d may be obtained using the Smoluchowski equation, $k_d = 4\pi N r_{D+A} D_{D+A}/1000$, where N is Avogadro's number, r_{D+A} is the effective encounter radius, and D_{D+A} is the mutual diffusion coefficient. Because encounter involves interaction in a cage slightly larger than the contact radius, we used an average $r_{D+A} = r_0 + 0.5$ Å or 6.5 Å in our evaluations. For low-viscosity solvents D_{D+A} may be estimated from the Stokes−Einstein equation, $D_{D+A} = D_D + D_A = (RT/6\pi\eta r_D N + RT/6\pi\eta r_A N)$, where R is the gas constant (8.31×10^7 erg deg^{-1}) and η is the viscosity in poise (g cm^{-1} s^{-1}). Using $\eta = 0.004$ poise and $r_D = r_A = 3.5$ Å yields $D_{D+A} = 2.5 \times 10^{-5}$ cm^2 s^{-1} and $k_d = 1.5 \times 10^{10}$ M^{-1} s^{-1} at 295 K. Because r_{D+A} appears in the numerator while r_D and r_A appear in the denominator in the calculation of k_d, the value is not particularly sensitive to the choice of these related parameters.

A value for k_{-d} may be statistically estimated from the equilibrium constant, K_{DA}, for the encounter complex.[30] According to ref 30 $k_d/k_{-d} = K_{DA} = [DA]/[D][A] = n/[S]$, where n is the coordination number of solvent molecules and [S] is the molar solvent concentration. For ethyl acetate [S] = 10 M. With n taken as 6, $k_d/k_{-d} = 0.6$ and $k_{-d} = 2.5 \times 10^{10}$ s^{-1}, which is the value that we used to calculate k_{et} in eq 9.[31] Substitution of $k_{en} = 7 \times 10^9$ M^{-1} s^{-1}, $k_d = 1.5 \times 10^{10}$ M^{-1} s^{-1}, and $k_{-d} = 2.5 \times 10^{10}$ s^{-1} into eq 9 yields $k_{et} = 2.2 \times 10^{10}$ s^{-1}.

To estimate k_0, eq 7 may be rearranged to eq 10

$$k_0 = k_{et} \exp[2(r_{D+A} - r_0)/L] \quad (10)$$

While the best values for L and k_0 were ultimately determined by fitting our experimental triplet energy-transfer data, prior studies have indicted that an L value of ~1 Å is typical for organic molecules.[12,13] With $r_0 = 6$ Å, $r_{D+A} = 6.5$ Å, and $L = 1$ Å, we obtained $k_0 = 6 \times 10^{10} s^{-1}$, which corresponds to the rate of exothermic triplet energy transfer from ^{3}D to a molecule of A in physical contact. This k_0 is consistent with rate constants of $\sim 10^{11}$ s^{-1} obtained by direct picosecond measurements of triplet energy transfer to acceptor solvents in which ^{3}D is in contact with more than one solvent molecule.[32] Although the k_0 value most appropriate to triplet energy transfer in film will ultimately be determined below from the fitting of the experimental data, it is important that this best-fit value be consistent with the solution k_0 value whether or not energy transfer is diffusion limited.

3.3. Nearest-Neighbor (NN) Model for Triplet Energy Transfer. The nearest-neighbor (NN) model for expressing the rate of triplet energy transfer in rigid media consists of summing or integrating the statistical fractional contributions of the various nearest-neighbor separation distances according to eq 4 multiplied by the associated energy-transfer rate constants given by eq 7. In fluid solution the decay of ^{3}D in the presence of A following pulsed excitation proceeds by a combination of unimolecular decay with a rate constant of k_T plus bimolecular energy transfer to A with an effective rate constant of k_{en}[A] according to eq 11

$$[^3D]/[^3D]_0 = \exp[-(k_T + k_{en}[A])t] \quad (11)$$

where $[^3D]_0$ is the initial concentration of ^{3}D just after the pulse. According to the NN model, the analogous decay expression in rigid media is eq 12

$$[^3D]/[^3D]_0 = \int_{r=r_0}^{\infty} f(r,dr)\exp[-\{k_T + k(r)\}t] \quad (12)$$

where $f(r,dr)$ and $k(r)$ are defined in eqs 4 and 7, respectively. For sufficiently small dr, for example, successive 1 Å shells, the integral in eq 12 may be replaced by a summation.

Equation 12 is somewhat similar to an expression derived previously by Inokuti and Hirayama neglecting excluded shell volume and total volume.[11] The latter expression was integrated to yield a series expansion, which may be truncated at $t > 10/k_0$. Subsequently, Rikenglaz and Rozman[33] and Hara and Gondo[15] derived analogous truncated series solutions that allowed for exclusion shells of radius r_0. The same model has also been applied to electron transfer in rigid media.[19]

While eq 12 or an analogous discrete summation can be applied to the decay of ^{3}D, we required an expression for the buildup of ^{3}A, which provided greater sensitivity in our experiments due to the high extinction coefficients and long lifetimes (τ_A) of suitable ^{3}A. In solution with sufficient excess A the buildup of ^{3}A following pulsed excitation of ^{3}D is given by eq 13

$$[^3A]/[^3D]_0 = \{k_{en}[A]/(k_{en}[A] + k_T - k_A)\}\{\exp(-k_A t) - \exp(-(k_T + k_{en}[A])t)\} \quad (13)$$

where k_A is the unimolecular decay constant ($1/\tau_A$) of ^{3}A. In a polymer film or other rigid medium in which diffusion does not occur and there is a distribution of D/A NN separations the analogous expression to eq 13 is eq 14

$$[^3A]/[^3D]_0 = \int_{r=r_0}^{\infty} f(r,dr)\{k(r)/[k(r) + k_T - k_A]\} \times \{\exp(-k_A t) - \exp(-[k_T + k(r)]t)\} \quad (14)$$

where $f(r,dr)$ and $k(r)$ are again defined by eqs 4 and 7, respectively. Integration of eq 14 is not simple, and a series solution is the likely result. On the other hand, eq 14 may be rewritten in terms of small Δr increments, representing successive spherical shells around ^{3}D, whose NN contributions can be numerically summed in a straightforward manner. In incremental form eq 14 becomes eq 15

$$[^3A]/[^3D]_0 = \sum_{r=r_0}^{\infty} f(r,\Delta r)\{k(r)/[k(r) + k_T - k_A]\} \times \{\exp(-k_A t) - \exp(-[k_T + k(r)]t)\} \quad (15)$$

where $f(r,\Delta r)$ with r in angstroms is given by eq 16

$$f(r,\Delta r) = 0.00756 r^2 [A]' \exp\{-0.00252(r^3 - r_0^3)[A]'\}\Delta r \quad (16)$$

Equation 15 is essentially exact if Δr is sufficiently small. This model recognizes the diversity of environments for various ^{3}D molecules and assigns appropriate energy-transfer rates based on the diverse D/A nearest-neighbor separation distances. We will subsequently show that it is the NN interactions that dominate exchange energy transfer in rigid media. The NN dominance reflects the rapid falloff in $k(r)$ in shells further removed than the NN shell. For example, with 1 Å spherical shells and $L = 1$ Å, $k(r)$ falls off 7.4-fold for each shell further removed than the NN shell according to eq 7.

In practice, application of eq 15 involves simply calculating and summing the fractional contributions of each NN shell. It was sufficient to use 1 Å Δr increments with the initial r radially centered in the first shell. For $r_0 = 6$ Å, the shell r values to be summed started at 6.5 Å and continued until contributing terms became negligible. For our calculations, the summations were typically carried out to about 14.5 Å. Values for $k(r)$ began at $r = 6.5$ Å for which $k(r) \approx k_{et}$ ($\sim 2.2 \times 10^{10}$ s^{-1}), the energy-transfer rate constant for a solution encounter complex with $r_{D+A} = 6.5$ Å. The summations were carried out at various times to generate kinetic plots for the buildup of ^{3}A.

3.4. Nearest-Neighbors (NNs) Models for Triplet Energy Transfer. In this section the NN model is refined by including the additional small contributions to energy transfer from NN shells in which more than a single A is centered and from A molecules centered in shells further removed than the NN shell. This will be referred to as the NNs model. The differential Perrin expression provides the probability, $f(r,dr)$, of finding one or more NN A in a shell of thickness dr centered at a separation between ^{3}D and A centers of r. In a small number of cases the NN shell will contain more than one A as determined by probability considerations. The appropriate $k(r)$ for each NN shell will increase in proportion to the A occupancy. It is possible to calculate the fractions of single and multiple occupancy shells and then sum their individual contributions to overall energy transfer. The calculations utilize the expression for, P_m, the probability that m particles out of a total of n particles are in a volume element, v, of a total volume, V, which is given by eq 17

$$P_m = S_{mn}(v/V)^m(1 - v/V)^{n-m} \quad (17)$$

where $S_{mn} = n!/[(n - m)!m!]$ is the number of possible m-particle combinations of n particles. It can be shown (see

Supporting Information) that the NNs model leads to eq 18 for $k'(r)$, the effective overall $k(r)$ as a function of [A], that can be used instead of $k(r)$ in eq 15

$$k'(r) = k(r)\{2 - [0.00756[\mathrm{A}]r^2 \exp(-0.00756[\mathrm{A}]r^2)/(1 - \exp(-0.00756[\mathrm{A}]r^2))]\} \quad (18)$$

The corrections to $k(r)$ due to multiple NN shell occupancy are generally small. For example, even at [A] = 0.4 M, the corrected $k'(r)$ is only about 15% higher than $k(r)$, roughly equivalent to selecting a 15% higher value for k_0.

At higher [A] there is a significant probability that the next closest shell to a NN shell will also contain one or more molecules of A, which may contribute to energy-transfer rates and efficiencies. To apply a correction to $k(r)$ for adjacent A-containing shells we calculated the fraction, f′, of NN shells at r that have A centered in adjacent shells and multiplied this fraction by $k(r + \Delta r)$. The fraction, f′, is just $v_{r+\Delta r}/V$. With r in angstroms and $\Delta r = 1$ Å, f′ is given by eq 19 (see Supporting Information).

$$\mathrm{f}'(r+1,1) = 0.00756(r+1)^2[\mathrm{A}] \quad (19)$$

By the same type of analysis that was applied to the NN shell it can be shown that the large majority of the occupied adjacent shells contain only a single A molecule, such that higher occupancies may be neglected. The net corrected rate constant, $k(r)_c$, that includes the contributions of energy transfer to NN shells containing more than one A and NN shells that contain another A in the next closest shell is given by eq 20

$$k(r)_c = k'(r) + \mathrm{f}'k(r+1) \quad (20)$$

Because $k(r + 1)$ is nearly an order of magnitude less than $k(r)$ or $k'(r)$ due to the exponential falloff (eq 7) and f′ is generally ≤ 0.3 for [A] ≤ 0.4 M and $r \leq 9$ Å (eq 19), f′$k(r + 1)$ is usually no more than a few percent of $k'(r)$ and the occupied adjacent shell correction is generally very small.

3.5. Medium-Constrained (MC) D/A Distribution. Up to this point the energy-transfer model has been based upon the assumption of a purely random and continuous distribution of D and A. However, there are at least two reasons these conditions may not be met. The first is D/A association, which would lead to a nonrandom distribution. As will be shown below, the observed concentration dependence of the energy-transfer efficiency follows Perrin-type probability behavior, which argues against formation of ground-state D/A complexes in our experiments.

A noncontinuous distribution can result from positioning constraints imposed by the molecules of the medium. D and A cannot simply assume any separation distance because, for the most part, the spaces between them must be occupied by molecules of the medium. The free volume of the medium, which is on the order of 30% for a liquid-like ethyl acetate,[34] provides some flexibility in this regard. For pure polymers, however, free volumes are typically only a few percent at the glass transition temperature (T_g) and somewhat less below T_g.[35] Local free volumes may be somewhat greater in the immediate vicinity of D or A dissolved in a polymer, but the surrounding polymer will still restrict this free space. Thus, the separations between D and A, while statistically driven, must occur approximately in multiples of the local dimensions of the medium. Those D and A not in contact will tend to be separated by at least the smallest dimension of the molecules comprising the medium, ~3−6 Å for an intervening polymer chain or side group. Thus, there will tend to be a scarcity of D/A in separations just beyond the inner shells in our NN or NNs models due to exclusion by molecules of the medium. This will tend to be compensated for by more in-contact r values and increases in the number of D/A separations just beyond those excluded by molecules of the medium. The f(r,Δr) values may be increased in the first two or three shells for which the r values may be considered to correspond to various contact orientations of nonspherical D/A molecules. For very large separations, which are less important for exchange energy transfer, the distributions will tend to be effectively continuous. The distribution constraints imposed by the molecules of the medium have been considered previously.[36] We explicitly considered this effect by including weighted f(r,Δr) values in a medium-constrained (MC) version of our analyses.

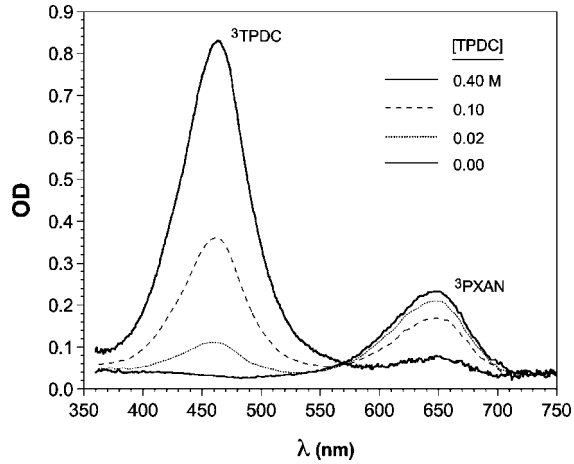

Figure 2. Transient T−T absorption spectra measured 5 μs after laser excitation at 343 nm of Ar-purged PMMA films with 0.026 M PXAN and 0.00, 0.02, 0.10, or 0.40 M TPDC.

4. Results and Discussion

4.1. T−T Absorption Spectra vs [A]. As noted above, polyphenyl derivatives can facilitate measurement of triplet energy transfer due to their high extinction coefficients for T−T absorption. The acceptor dibutyl-3,3′-terphenyldicarboxylate (TPDC), which has a triplet energy of 60.5 kcal/mol,[22a] proved particularly useful due to its high solubility in PMMA. 2-*tert*-Pentylxanthone (PXAN) served as a suitable triplet energy donor due to its higher triplet energy of 70.3 kcal/mol[22a] and strong absorption at the laser excitation wavelength of 343 nm, where TPDC is transparent. Transient T−T absorption spectra of approximately 25 μm thick argon-purged PMMA films containing 0.026 M PXAN with 0.00, 0.02, 0.10, and 0.40 M TPDC are shown in Figure 2. These spectra were measured at 5 μs after the laser excitation pulse, at which time the absorbance of ^{3}TPDC had almost maximized in all films (see below). Nearly all of the ^{3}PXAN quenching that ultimately occurred took place within 5 μs with minimal ^{3}TPDC decay. Thus, the ^{3}TPDC optical densities in Figure 2 provided a direct measure of the approximate quantum efficiencies of triplet energy transfer, Φ_{T-T}, for the three TPDC concentrations. The optical densities of ^{3}TPDC at the λ_{max} of 460 nm corrected for absorption due to ^{3}PXAN are 0.08, 0.33, and 0.82 for 0.02, 0.10, and 0.40 M TPDC, respectively. Both the data in Figure 2 and independent measurements indicated that the extinction coefficient at λ_{max} of ^{3}TPDC is approximately five times that of ^{3}PXAN in PMMA. This allowed quantum yields for triplet energy transfer (Φ_{T-T}) of 0.07, 0.29, and 0.71 to be determined for 0.02, 0.10, and 0.40 M TPDC, respectively, from the ^{3}TPDC OD values relative to the initial ^{3}PXAN OD at 650 nm with no TPDC. As will be

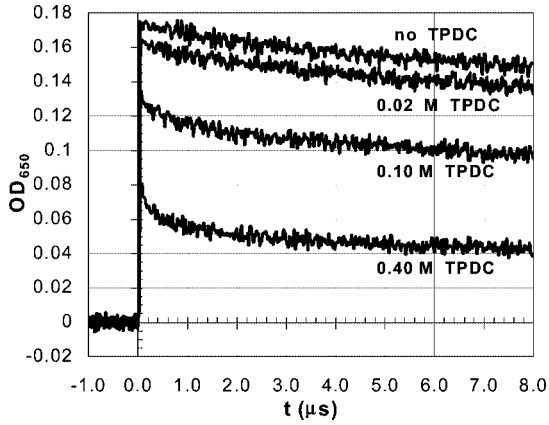

Figure 3. Decay of ^{3}PXAN OD at 650 nm following laser excitation of argon-purged PMMA films containing donor PXAN and acceptor TPDC at (a) 0.00, (b) 0.02, (c) 0.10, and (d) 0.40 M.

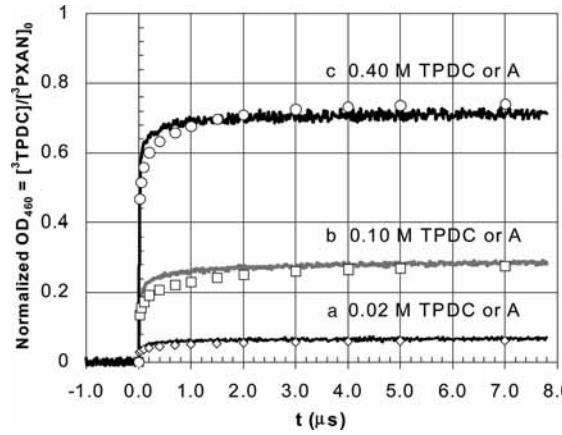

Figure 4. Buildup of ^{3}TPDC OD at 460 nm (lines) following laser excitation of argon-purged PMMA films containing donor PXAN and acceptor TPDC at (a) 0.02, (b) 0.10, and (c) 0.40 M and simulated buildup of ^{3}A via triplet energy transfer (points) according to NN eq 15 following pulsed laser excitation of D for (a) 0.02, (b) 0.10 (b), and (c) 0.40 M A with $k_0 = 7.7 \times 10^{10}$ s^{-1}, $r_0 = 6$ Å, $L = 0.8$ Å, $k_T = 2 \times 10^4$ s^{-1}, and $k_A = 4 \times 10^3$ s^{-1}.

shown below, both the ratios and absolute Φ_{T-T} values are consistent with a Dexter exchange energy-transfer mechanism involving a Perrin-type distribution of D/A separation distances as described by eq 15.

Importantly, the ^{3}TPDC ratios in Figure 2 are inconsistent with those that would be expected based solely on ground-state association of PXAN and TPDC. If the observed ^{3}TPDC yield of 0.71 at 0.40 M TPDC were due to full energy transfer from ^{3}PXAN to associated TPDC molecules, then the association constant would be about 1.8 M^{-1}. This would lead to predicted ^{3}TPDC yields for 0.02 and 0.10 M TPDC of only 0.036 and 0.18, whereas the experimental yields were 0.07 and 0.29, respectively.

4.2. Decay of ^{3}D vs [A]. The decay of the T−T absorption of ^{3}PXAN in the argon-purged films of Figure 2 produced by laser pulses of constant energy is shown in Figure 3. The ^{3}PXAN absorption was measured at 650 nm, where ^{3}TPDC absorption is negligible. In the absence of TPDC, k_T for ^{3}PXAN was approximately 2×10^4 s^{-1} over the time scale of these measurements. As is clear from Figure 3, the primary effect of added TPDC was to reduce the amount of ^{3}PXAN at times of <0.1 μs. Some additional increase in the rate of decay of ^{3}PXAN was evident between approximately 0.1 and 2.0 μs, particularly at higher [TPDC]. However, by about 5 μs the ^{3}PXAN decay rate became very similar in all four samples. At 5 μs the ^{3}PXAN OD was reduced by about 7%, 31%, and 72% for 0.02, 0.10, and 0.40 M TPDC, respectively, similar to the Φ_{T-T} ratios noted above. Due to the combination of pulse intensity variability and noise, ^{3}PXAN decay plots like those in Figure 3 were not ideally suited to the quantitative determination of energy-transfer rates. This was particularly true at low TPDC concentrations, where it was difficult to precisely measure the small reductions in the ^{3}PXAN signals. More reliable results were obtained from the buildup of 3TPDC, as described below.

4.3. Buildup of ^{3}A vs [A]. Because there is very little ^{3}PXAN absorption at 460 nm, the kinetics of buildup of OD at 460 nm due to ^{3}TPDC formation provided a relatively clear indication of the kinetics of energy transfer to TPDC, even at low TPDC concentrations. Kinetic plots of the OD buildup at 460 nm were also less noisy due the very high extinction coefficient of ^{3}TPDC and the high detector sensitivity at 460 nm. The experimental data for the argon-purged, TPDC-containing films of Figures 2 and 3 are shown by the lines in Figure 4. Laser excitation of a PMMA film containing TPDC without PXAN produced no ^{3}TPDC absorption due to the transparency of TPDC at a laser wavelength of 343 nm. Again, it is evident that most of the energy transfer has taken place in <0.1 μs but with significant additional buildup between about 0.1 and 2.0 μs. The level of ^{3}TPDC nearly reached a plateau at ~5 μs in these films and then decayed slowly ($\tau \approx 0.3$ ms) at longer times. The optical densities of Figure 4 have been normalized such that an OD of unity corresponds to $\Phi_{T-T} = 1.0$. From the plateau values of the lines in Figure 4, Φ_{T-T} values of 0.07, 0.28, and 0.72 were estimated for 0.02, 0.10, and 0.40 M TPDC, respectively. A very small correction has been applied to the data to compensate for the slight decay in absorption of ^{3}PXAN at 460 nm. Examples of the kinetics of ^{3}A buildup at shorter times are provided below and in the Supporting Information.

Other donors such as DETX yielded kinetic plots very similar to those in Figure 4, as did other polyphenyl acceptors, including PTP and BPDC, studied at 0.10 M, and also naphthalene derivatives, such as methyl-1-naphthalene acetate (see below). Kinetic plots of ^{3}PTP buildup were also similar in other polymer films, including low-T_g poly(ethyl methacrylate) and poly(vinylidene chloride coacrylonitrile) (Saran F-310) and high-T_g cellulose acetate butyrate (30% acetyl, 17% butyryl) and polycarbonate films.

4.4. Theoretical Results: ^{3}A Formation Kinetics and Yields. In this section we explore the ability of the nearest-neighbor (NN) and nearest-neighbors (NNs) models and the medium-constrained (MC) modification presented in sections 3.3−3.5 to reproduce the experimental energy-transfer behavior represented by the lines in Figure 4.

4.4.1. NN Analysis. An attempt to reproduce the experimental kinetics of ^{3}A buildup shown by the lines in Figure 4 by applying the NN model, and eq 15 is shown by the points in Figure 4. For these simulations $k_0 = 7.7 \times 10^{10}$ s^{-1}, $r_0 = 6$ Å, $L = 0.8$ Å, $k_T = 2 \times 10^4$ s^{-1}, and $k_A = 4 \times 10^3$ s^{-1}, with k_0 and L having been adjusted to fit the data. The calculated $[^3A]/[^3D]_0$ points in Figure 4 approach plateaus that are equivalent to Φ_{T-T} values and similar to the experimental values, providing support for the Perrin-type random distribution model. However, the ^{3}A buildup in the first few microseconds in the simulations is clearly more gradual than the experimental buildup.

The summations (eq 15) used to generate the simulations in Figure 4 were carried out in 1 Å Δr increments beginning at a shell centered at $r = 6.5$ Å with a $k(6.5\text{ Å})$ of 2.2×10^{10} s^{-1}, the same as estimated above from the solution energy-transfer

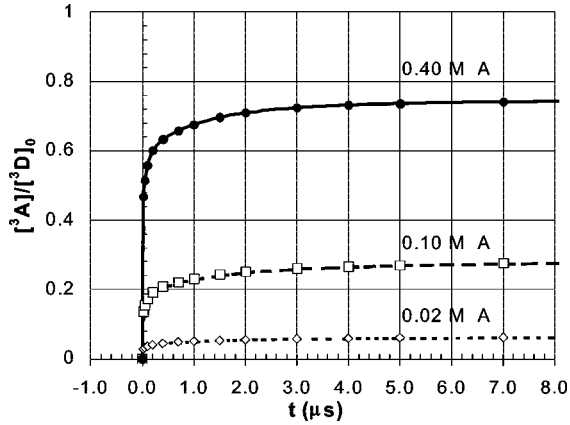

Figure 5. Lines show the buildup of ^{3}A via triplet energy transfer according to the NNs model (eq 15 but with $k(r)_c$ of eq 20) following pulsed laser excitation of D for (a) 0.02, (b) 0.10, and (c) 0.40 M A with $k_0 = 6.3 \times 10^{10}$ s^{-1}, $r_0 = 6$ Å, $L = 0.8$ Å, $k_T = 2 \times 10^4$ s^{-1}, and $k_A = 4 \times 10^3$ s^{-1}. Points are from the NN model (eq 15) with the same parameters as in Figure 4 for comparison.

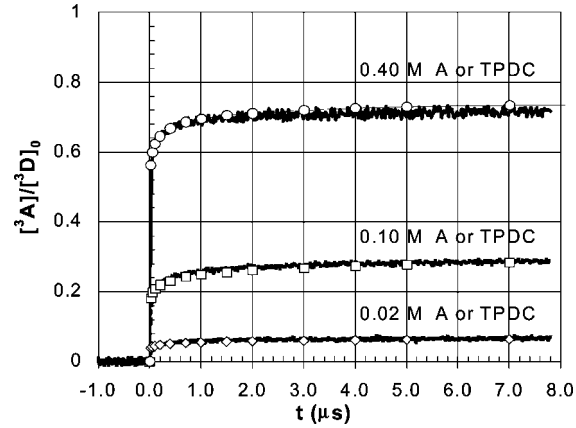

Figure 6. Points show the buildup of ^{3}A via triplet energy transfer according to the MC NNs model following pulse excitation of D for (a) 0.02, (b) 0.10, and (c) 0.40 M A with $k_0 = 9.7 \times 10^{10}$ s^{-1}, $r_0 = 6$ Å, $L = 0.85$ Å, $k_T = 2 \times 10^4$ s^{-1}, and $k_A = 4 \times 10^3$ s^{-1} and the MC redistributions noted in the text. The lines repeat the experimental data of Figure 4.

data. This corresponds to a k_0 of 7.7×10^{10} s^{-1} at the r_0 of 6 Å with $L = 0.8$ Å. Summations were carried out to $r = 14.5$ Å, beyond which quenching contributions were negligible. The simulated ^{3}A buildup yielded a slightly better fit to the experimental data with a smaller L value (e.g., 0.7 Å) along with a larger k_0 (3.3×10^{11} s^{-1}). However, a significantly smaller L is not very realistic based on previous analyses or on the nature of the interacting orbitals.[12,13,27] Slightly larger L values combined with smaller k_0 values were also found to match experimental plateau levels reasonably well but gave a worse fit to the buildup of ^{3}A.

4.4.2. NNs Analysis. For the simulation shown in Figure 5 the full NNs model was used, consisting of eq 15 plus $k(r)_c$ as defined by eq 20. Without changing any of the parameters the NNs model yielded $[^3A]/[^3D]_0$ plateau values that are slightly higher than those of the NN model due to the contributions to $k(r)_c$ from NN shells with more than one A molecule and from additional energy transfer to A molecules centered in shells just beyond the NN shell (data not shown). However, as shown in Figure 5, the NNs model provided simulations that are nearly identical to those of the NN model of Figure 4 if k_0 was reduced by about 18% to 6.3×10^{10} s^{-1}. The lines in Figure 5 represent the NNs simulations with $k_0 = 6.3 \times 10^{10}$ s^{-1}, $r_0 = 6$ Å, $L = 0.8$ Å, $k_T = 2 \times 10^4$ s^{-1}, and $k_A = 4 \times 10^3$ s^{-1}. The points are taken from the NN simulation of Figure 4 with $k_0 = 7.7 \times 10^{10}$ s^{-1} and the other parameters unchanged. Neither of these fits reproduces the early buildup of ^{3}A particularly well.

Interestingly, comparisons of calculated NN $[^3A]/[^3D]_0$ values to NNs $[^3A]/[^3D]_0$ values with the same parameters indicated that >90% of quenching of ^{3}D is due to energy transfer to A centered in a NN shell containing a single A molecule for [A] ≤ 0.4 M. Furthermore, a comparison of calculated $[^3A]/[^3D]_0$ values indicated that energy transfer to A molecules centered in the shell just beyond the NN shell (the $f'k(r+1)$ term in eq 20) contributes <3% to the overall triplet energy transfer. Thus, to a very large extent (>∼85%) energy transfer from ^{3}D to ≤0.4 M A involves the interaction between ^{3}D and a single nearest-neighbor A molecule in our experiments.

A limited number of simulations were carried out in which the fractions of multiple occupancy NN shells and NN shells with another A in the adjacent shell were calculated separately and explicitly included in summations according to eq 15. The results were indistinguishable from those obtained by treating these two components of the probability distribution in terms of their contributions to an effective $k(r)_c$, as noted in section 3.4.

4.4.3. Medium-Constrained (MC) NNs Analysis. As is evident from Figures 4 and 5, the NN and NNs models yield somewhat less ^{3}A at very short times and greater ^{3}A formation in the 0.2−3.0 μs time range than was observed experimentally. Although the NN and NNs model can provide nearly identical results with a slight adjustment of k_0 values, we used the conceptually more correct NNs model for subsequent simulations. Qualitatively, the kinetic data could be explained if, compared to the statistical NNs model, additional A molecules were concentrated in the few 1 Å shells nearest to ^{3}D (for which $k(r)$ values are very large) and fewer A molecules were located in the next few shells (for which $k(r)$ values are in neighborhood 10^6 s^{-1}). Such a redistribution would be expected according to the MC model because molecules of the medium would tend to physically exclude D/A separations in the $r \approx [r_0 + (3-6)]$ Å range. To compensate, $f(r,\Delta r)$ values would tend to increase in the first few shells for which the r values correspond to various orientations of nonspherical D/A molecules in physical contact as well as for shells just beyond $\sim(r_0 + 6)$ Å.

For the simulation in Figure 6, 40% of the A molecules centered in the fourth (r_0 + 3−4 Å) shell of the NNs model were distributed equally between the first (r_0 + 0−1 Å) and seventh (r_0 + 6−7 Å) shells and similarly 40% of the A molecules in the fifth (r_0 + 4−5 Å) and sixth (r_0 + 5−6 Å) shells were distributed equally between the second and eighth and third and ninth shells, respectively. This redistribution model resulted from numerous attempts to better fit the experimental data by taking into account the tendency of the molecules of the medium to physically exclude D/A separations in the 3−6 Å range. This method also ensured that $f(r,\Delta r)$ values still summed to unity. As noted above, the r values for the first three shells were taken to reflect nonspherical D and A molecules in direct contact at various orientations. The pattern of redistribution of A molecules from the fourth through sixth shells into the other six shells reflects the proportional volumes of the various shells. For larger separations ($r > r_0 + 9$ Å) many configurations are possible, and the distributions will tend to follow the simple NNs model.

The points in Figure 6 represent the results of a simulation according to the MC NNs model. The NNs parameters were k_0

$= 9.7 \times 10^{10}$ s^{-1} (corresponding to a k of 3.0×10^{10} s^{-1} in the center of the first shell), $r_0 = 6$ Å, $L = 0.85$ Å, $k_T = 2 \times 10^4$ s^{-1}, and $k_A = 4 \times 10^3$ s^{-1}. Here the MC redistributions noted above were included to adjust the f(r,Δr) values and effective A occupancies in the first nine shells. For the fitting, the k_0 and L values were maintained close to those of the pure NNs model, which provided reasonable plateau $[^3A]/[^3D]_0$ values. Importantly, inclusion of medium constraints provided a much improved fitting to the short-time kinetic data. The agreement between the simulations and experimental data is quite good, especially considering the relative simplicity of the redistribution procedure. The predicted plateau $[^3A]/[^3D]_0$ value at 0.40 M A is very slightly high in the simulation relative to the values at the lower concentrations, although this is within the experimental variability of a few percent. The small difference between experiment and theory may also reflect the possibility that for the relatively high ^{3}A optical densities monitored at 0.40 M A, a slight departure from Beer's law may have occurred due to inhomogeneities in the laser beam. While other more complicated MC redistribution patterns may also fit the experimental data, this relatively simple example served to illustrate the concept.

The f(r,Δr) distribution corrections used for the MC model above are qualitatively similar to the distributions of molecular separations in pure liquids and glasses that are expressed by so-called radial distribution functions.[37] Radial distribution functions have also been determined for noncrystalline polymers, including PMMA.[38] These reflect a localized order in molecular separations arising primarily from repulsive forces. Due to the limited free volume, molecular separations in pure liquids tend to occur in integral multiples of the molecular dimensions, i.e., molecules tend to be nearly close packed. Similar restrictions apply in liquid or solid solutions like our polymer films, where the molecules of the medium tend to physically control the likely separations of dissolved components. Because of this, r distributions are not purely continuous at close separations. An alternative analysis of exchange energy transfer along somewhat similar lines has been provided by Blumen,[39] who considered energy transfer in terms of a lattice arrangement of D and A molecules.

Finally, we note that the buildup in T−T absorption at 460 nm upon direct excitation of TPDC with 308 nm laser pulses was ∼98% complete in 100 ns. This ruled out the possibility of slow nuclear reconfiguration of ^{3}TBDC as a contributory factor in the delayed buildup of the optical density between 0.2 and 2 μs shown in Figures 4 and 6.

The buildup of ^{3}A according to the NNs and MC NNs models with longer lived ^{3}D ($\tau_T = 1$ ms) and ^{3}A ($\tau_A = 10$ ms) is illustrated in the Supporting Information. Even with the longer triplet lifetimes the large majority of ^{3}A ultimately produced is formed within the first few microseconds after pulsed excitation of D.

4.5. Additional Experimental Data and Discussion. As noted previously, other donors and acceptors with similar energetic relationships resulted in similar kinetic plots of triplet energy transfer in PMMA. The buildup of optical density at 425 nm due to energy transfer from ^{3}PXAN to 0.10 M methyl-1-naphthalene acetate (M1NA) ($E_T = 59.5$ kcal/mol)[22a] in PMMA is shown by the points in Figure 7. A line plot of the buildup in optical density at 460 nm with 0.10 M TPDC is included for comparison. The results are clearly very similar for the two acceptors.

A limited number of energy-transfer measurements were performed in other polymer films, most of which were more difficult to coat. A comparison of the kinetics of energy transfer from ^{3}PXAN to 0.10 M PTP in PMMA and cellulose acetate butyrate (CAB) is provided in the Supporting Information.

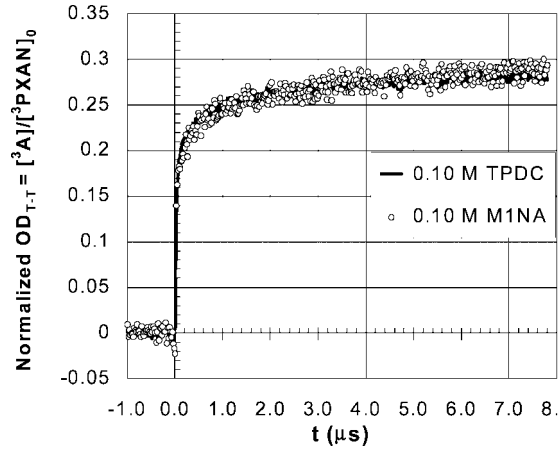

Figure 7. Buildup of ^{3}A OD following laser excitation of argon-purged PMMA films containing donor PXAN and (a) 0.10 M acceptor TPDC (monitored at 460 nm, line) and (b) 0.10 M M1NA (monitored at 425 nm, points) corrected for 3PXAN OD changes and normalized to yield $[^3A]/[^3PXAN]_0$.

The ^{3}A formation kinetics exemplified by the plots in Figures 4 and 6 and the plot for CAB in the Supporting Information appear bimodal in nature with a rapid (≤0.1 μs) initial formation of approximately 75% of the final yield of ^{3}A followed by a transition period and then a more gradual ^{3}A buildup from roughly 0.5 to 20 μs, which is most evident when k_T is small. The initial rapid buildup may be attributed to energy transfer to A molecules in physical contact with ^{3}D at various orientations, the transition presumably reflects the scarcity of r separations in the $r_0 + (3-6)$ Å range due to exclusion by polymer molecules in contact with ^{3}D, and the smaller gradual buildup at longer times may be attributed to energy transfer to A molecules just beyond the D/A separations excluded by polymer.

Both molecular size considerations and the nonexponential buildup of ^{3}A in plots like those in Figures 4, 6, and 7 suggest the need to consider medium-induced restrictions in D/A separations similar the discrete site model of Suppan et al.[36] However, the conclusion of Suppan and co-workers that ^{3}D and A must be in van der Waals contact for triplet energy transfer or electron transfer is unnecessarily restrictive. The significant buildup in ^{3}A that occurs in the 0.5−20 μs range is too slow to be explained by energy transfer between ^{3}D and A in contact. Other studies have also observed substantial triplet energy transfer on the microsecond time scale.[13,20] According to the Dexter expression, $k(r)$ will be in the neighborhood of 6×10^5 s^{-1} when $r \approx (r_0 + 6$ Å) with $k_o = 10^{11}$ s^{-1} and $L = 1$ Å. The medium, e.g., PMMA, may promote such D/A separations (see Figure 7), and it is entirely reasonable to attribute the buildup of ^{3}A in the microsecond time regime to exchange energy transfer from ^{3}D to A at $r \approx (r_0 + 6$ Å).

Suppan et al. propose two alternative explanations for slower triplet energy transfer.[36] The first is that molecular motions may increase D/A separation in the lifetime of ^{3}D. However, the lack of free volume and the high T_g of polymers like PMMA would not allow sufficient translational motion on a microseconds time scale, and it is unclear how such displacement would be functionally different than a larger initial separation. Second, a long-range Coulombic dipole−dipole process is offered as a possible explanation for slower triplet energy transfer. This

might be a possibility at millisecond or greater time scales, particularly if n−π* triplet states are involved or if D and/or A possess heavy atoms.[40] However, for the highly forbidden S−T transitions of the molecules in our study, which lack substantial spin−orbit coupling, Coulombic transfer rates are many orders of magnitude below the 10^5-10^6 s^{-1} rates observed.[41]

The fitting of our experimental data with the MC NNs model (see Figure 6) provided very reasonable values for L of ∼0.85 Å and k_0 of $\sim 10^{11}$ s^{-1}. L is similar to a recent theoretical determination of about 0.8 Å,[27] and k_0 is similar to the estimate from solution data above.[42] Allowing for uncertainty in the exact perturbation of D/A separations by the medium, the true L may be in the range of approximately 0.75−0.95 Å. Prior analyses of triplet energy transfer in rigid media have yielded a wide range of L and k_0 values. This is exemplified by the data in Table 1 of ref 13, where k_0 is referred to as k_v and spans a range from $\sim 10^4$ to 10^{16} s^{-1}. Most of the k_0 (k_v) values in Table 1 are $\leq 10^8$ s^{-1},which are inconsistent with the nearly diffusion-limited rates of exothermic triplet energy transfer routinely measured in solution.[29] The low k_0 determinations typically involved analyses of long-lived triplets at relatively long times, which largely probed energy transfer only from ^{3}D molecules that have nearest-neighbor A molecules that are relatively distant. Aside from the factors that the models used in some of these analyses are less exact than the NNs model and that medium constraints were not considered, the low k_0 results may also reflect the possibility that over long distances the falloff in $k(r)$ is not simply exponential. This might not be surprising for transitions involving π orbitals in nonspherical molecules. It was previously suggested[13,20] that the effective $k(r)$ for exchange energy transfer may increase more rapidly with decreasing r than expressed by eq 7. It is also possible that the k_0 appropriate for D and A in contact might not be applicable when electrons must tunnel through intervening molecules of the medium.[43] However, the MC NNs model was able to fit our experimental data out to $r \geq 15$ Å with a single reasonable value for k_0. Alternatively, for very long-lived triplets that transfer energy over longer distances, resonance triplet energy transfer may convolute analysis.[40] It should be noted that pulse measurements that have probed triplet energy transfer at shorter times have tended to yield results more similar to those of this study.[13,45] The L values previously obtained for organic triplets range from ∼0.7 to 2.1 Å.[13,15] These differences have a profound effect on $k(r)$ due to the exponential dependence on L (eq 7).

Experimental data obtained for transfer of energy from ^{3}PXAN to 0.40 M TPDC in PMMA at a time scale limited by the resolution of the nanosecond photolysis system are provided in Figure 8. A simulation using the MC NNs model with the parameters of Figure 6 is included for comparison, and the agreement is reasonably good. The poorer fit between the model and the experimental data in the first 30 ns reflects the laser pulse width (∼7 ns) plus the slow response of the electronics. We also performed a limited amount of triplet energy-transfer measurements using a picosecond laser photolysis system. While noisy, these data indicated that ∼50% of the energy transfer from ^{3}PXAN to 0.4 M TPDC occurred within 1 ns, which is consistent with the model.

5. Additional Applications

5.1. ^{3}AYields and Φ/Φ^0 Calculations for NNs vs Perrin Models. When the lifetimes of ^{3}A products are long relative to those of ^{3}D, plateau values of plots of $[^3A]/[^3D]_0$ like those in Figures 5 and 6 provide ^{3}A NNs quantum yields. By analogy with solution quenching, it can be shown that the ratio of the

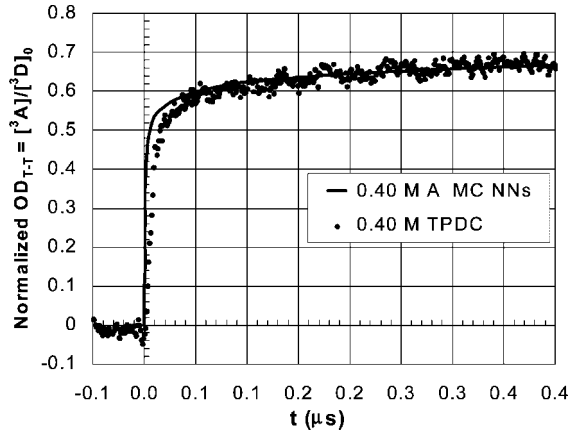

Figure 8. Experimental kinetics of ^{3}TPDC buildup (points) at 460 nm via energy transfer from ^{3}PXAN to 0.40 M TPDC in argon-purged PMMA vs the ^{3}A buildup (line) simulated using the MC NNs model with the parameters of Figure 6.

phosphorescence quantum yield, Φ_{ph}, of ^{3}D at a given [A] to that in the absence of A, Φ_{ph}^0, is related to the quantum yield of ^{3}A, Φ_{T-T}, by eq 21

$$\Phi_{ph}/\Phi_{ph}^{\ 0} = 1 - \Phi_{T-T} \tag{21}$$

Alternatively, in rigid media Φ_{ph}/Φ_{ph}^0 may be obtained from the NNs summation of eq 22

$$\Phi_{ph}/\Phi_{ph}^{\ 0} = k_T \sum_{r=r_0}^{r'} f(r,\Delta r)/[k_T + k(r)_c] \tag{22}$$

which is analogous to the solution expression for phosphorescence quenching of $\Phi_{ph}/\Phi_{ph}^0 = k_T/(k_T + k_{en}[A])$. The summation of eq 22 must be carried out to an r' at which $f(r',\Delta r) < 0.002$. Φ_{T-T} may then be calculated from eq 21. Simulations carried out using both methods (eq 22 or the plateau of eq 15) of determining Φ_{ph}/Φ_{ph}^0 yielded identical results.

According to the Perrin model with excluded contact volume, Φ_{T-T} is given by an expression of the form of eq 2. Referring to eq 21, Φ_{ph}/Φ_{ph}^0 is then obtained according to a Perrin model with excluded total volume from eq 23

$$\Phi_{ph}/\Phi_{ph}^{\ 0} = \exp\{-0.00252(r_c^3 - r_0^3)[A]'\} \tag{23}$$

NNs and Perrin simulations may be compared by finding a value for r_c in eq 23 that best reproduces the more exact NNs calculations obtained via eq 22 or alternatively via eq 15 (together with eq 21). The results of a representative comparison are provided in Figure 9. For the NNs simulation the parameters selected were $k_0 = 1.0 \times 10^{11}$ s^{-1}, $r_0 = 6$ Å, $L = 0.8$ Å, $k_T = 10^4 s^{-1}$, and $k_A < 10^2$ s^{-1}, and the results are shown by the solid (Φ_{ph}/Φ_{ph}^0) and dashed (Φ_{T-T}) lines in Figure 9. The filled points in Figure 9 are the best-fit Perrin results according to eq 23 for Φ_{ph}/Φ_{ph}^0 (squares) and eq 21 for Φ_{T-T} (triangles) with $r_0 = 6$ Å and $r_c = 12.45$ Å. The Perrin data points are remarkably close to the NNs curves, considering the simplicity of the Perrin model. If instead it is assumed that $r_0 = 0$ Å for the Perrin model, the NNs simulation can also be fit reasonably well, but an r_c of 12.2 Å is required. While this assumption is inappropriate, the error in r_c in this example is not too severe.

The Perrin model is usually considered to provide no kinetic information; rather it is typically interpreted as providing a critical separation, r_c, inside of which all ^{3}D are quenched and beyond which there is no quenching. However, when we substituted the best-fit r_c of 12.45 Å and the NNs k_0 of 1.0 ×

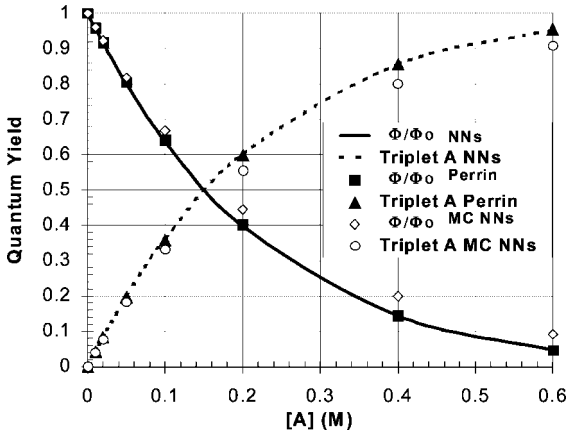

Figure 9. Quantum yields of ^{3}A formed by energy transfer and Φ/Φ^0 for phosphorescence of ^{3}D vs [A] simulated with the (a) NNs model (eq 22, lines), (b) best-fit Perrin model (eq 23, $r_c = 12.45$ Å, filled points), and (c) MC NNs model (open points). For the NNs models $k_0 = 1.0 \times 10^{11}$ s^{-1}, $r_0 = 6$ Å, $L = 0.8$ Å, $k_T = 10^4$ s^{-1}, and $k_A < 10^2$ s^{-1}. MC NNs redistributions are the same as for Figure 6.

10^{11} s^{-1} and L of 0.8 Å into eq 7, we obtained a value for $k(r_c)$ of 0.99×10^4 s^{-1}, which equals k_T. This indicates that the best-fit value of r_c obtained from a properly constructed Perrin model (with excluded contact and total volume) is actually the ^{3}D/A separation at which $k(r) = k_T$. If we instead used $r_0 = 0$ Å and the best-fit $r_c = 12.2$ Å, we obtained a meaningless $k(r_c)$ value (5.7×10^{-3}s^{-1}). Additional simulations showed that, in general, for quenching defined by eq 23, r_c is the separation at which the quenching rate constant equals the lifetime of the species quenched.

Also included in Figure 9 is a MC NNs simulation with ^{3}D/A separations redistributed as in Figure 6, i.e., with 40% of the f(r,Δr) from respective shells 4−6 redistributed equally among shells 1−3 and 7−9. This attempts to correct for the physical constraints of the molecules of the medium on the distribution of ^{3}D/A separations. It leads, in this case, to noticeable reductions in ^{3}D quenching and ^{3}A quantum yields (open points) relative to the NNs model at higher [A].

5.2. Application to Electron Transfer in Rigid Media. Photoinduced electron transfer in rigid media is analogous to triplet energy transfer except that instead of involving the exchange of two electrons only a single electron is transferred from donor to acceptor. The NNs model is applied to electron transfer and compared to earlier models in the Supporting Information.

6. Conclusions

A laser flash photolysis procedure has been used to study the kinetics of exothermic triplet energy transfer in polymer films via decay of triplet donor (^{3}D) absorption and buildup of triplet acceptor (^{3}A) absorption. For the materials investigated, most of the energy transfer occurred within the first 100 ns after the laser pulse. This was followed by a period of slower buildup from about 0.2 to 10 μs. Both the experimental kinetics and the ^{3}D quantum yields were reproduced reasonably well by a differential Perrin-type nearest-neighbors model modified to accommodate molecular volumes coupled with a Dexter-type exponential falloff in the electron-exchange rate constant, $k(r)$, with D/A separation distance, r. However, the experimental data were reproduced much more closely by including the effects of the physical constraints of the molecules of the polymer medium on the distribution of D/A separations. A comparison of NN and NNs models for triplet energy transfer indicated that under the conditions of these experiments the transfer of triplet energy from ^{3}D to A to a very large extent involves the interaction between ^{3}D and a single nearest-neighbor molecule. Fitting to the experimental data for exothermic energy transfer from ^{3}PXAN to TPDC in PMMA yielded a value for k_0, the rate constant for transfer of energy from ^{3}D and A in physical contact, of $\sim 10^{11}$ s^{-1} and an L value, describing the falloff in $k(r)$ with r in exp[2($r - r_0$)/L], of approximately 0.85 Å. The experimental kinetic data demonstrated that exchange energy transfer is not restricted to ^{3}D and A molecules in physical contact and that the k_0 value appropriate for the rigid polymer films is totally consistent with solution energy-transfer kinetics.

Quantum yields of ^{3}A calculated with the NNs and MC NNs models were also compared to values obtained with the simple Perrin model modified to include the effects of molecular volumes. The fits between the NNs and Perrin simulations were quite good, and it was shown that the best-fit Perrin r_c corresponds to the ^{3}D/A separation at which $k(r) = k_T$. At higher [A], both the NNs and Perrin simulations showed significant departures from the presumably more accurate MC NNs results.

Supporting Information Available: (I) Derivation of eq 18 for $k'(r)$, (II) derivation of $f'(r + 1,1)$, (III) plot of ^{3}PTP buildup at a short time scale, (VI) simulated ^{3}A buildup with small k_T and k_A, (V) triplet energy transfer in cellulose acetate butyrate, (VI) application to electron transfer in rigid media and comparison of the NNs model with the CV and RR models. This material is available free of charge via the Internet at http://pubs.acs.org.

Acknowledgment. This research was supported by the National Science Foundation (Grants CHE-0749919 and DMR-0071303). We thank Dr. Douglas Robello and Mr. Mark Mis of Eastman Kodak Co. for providing several donor and acceptor samples. We thank the reviewers for helpful comments.

References and Notes

(1) (a) Cogdell, R. J. *Philos. Trans. R. Soc. London B* **1978**, *284*, 569. (b) Rondonuwu, F. S.; Taguchi, T.; Fujii, R.; Yokoyama, K.; Koyama, Y.; Watanabe, Y. *Chem. Phys. Lett.* **2004**, *384*, 364.

(2) Laquai, F.; Wegner, G.; Im, C.; Büsing, A.; Huen, S. *J. Chem. Phys.* **2005**, *123*, 074902.

(3) (a) Baldo, M. A.; O'Brien, D. F.; You, Y.; Shoustikov, A.; Sibley, S.; Thompson, M. E.; Forrest, S. R. *Nature* **1998**, *395*, 151. (b) Baldo, M. A.; Forrest, S. R. *Phys. Rev. B* **2000**, *62*, 10958. (c) Kalinowski, J.; Stampor, W.; Cocchi, M.; Virgili, D.; Fattori, V.; Di Marco, P. *Chem. Phys.* **2004**, *297*, 39. (d) Baldo, M.; Segal, M. *Phys. Stat. Solidi A: Appl. Res.* **2004**, *201*, 1205.

(4) King, S. M.; Al-Attar, H. A.; Evans, R. J.; Congreve, A.; Beeby, A.; Monkman, A. P. *Adv. Funct. Mater.* **2006**, *16*, 1043, and references therein.

(5) Farid, S. Y.; Robello, D. R.; Dinnocenzo, J. P.; Merkel, P. B.; Ferrar, L. S.; Roh, Y.; Mis, M. U.S. Patent Application 2005136357 A1, June 23, 2005.

(6) (a) Closs, G. L.; Piotrowiak, P.; MacInnis, J. M.; Fleming, G. R. *J. Am. Chem. Soc.* **1988**, *110*, 2652. (b) Closs, G. L.; Johnson, M. D.; Miller, J. R.; Piotrowiak, P. *J. Am. Chem. Soc.* **1989**, *111*, 3751.

(7) (a) Thompson, B. C.; Frechet, J. M. J. *Angew. Chem., Int. Ed.* **2008**, *47*, 58. (b) Guo, F.; Kim, Y.-G.; Reynolds, J. R.; Schanze, K. S. *Chem. Commun.* **2006**, (17), 1887.

(8) Graetzel, M. *Inorg. Chem.* **2005**, *44*, 6841, and references therein.

(9) Durrant, J. R.; Haque, S. A.; Palomares, E. *Chem. Commun.* **2006**, (31), 3279, and references therein.

(10) Ermolaev, V. L. *Opt. Spect.* **1959**, *6*, 417.

(11) Inokuti, M.; Hirayama, F. *J. Chem. Phys.* **1965**, *43*, 1978.

(12) Strambini, G. B.; Galley, W. C. *J. Chem. Phys.* **1975**, *63*, 3467.

(13) Strambini, G. B.; Galley, W. C. *Chem. Phys. Lett.* **1976**, *39*, 257.

(14) Brown, A.; Wilkinson, F. *J. Chem. Soc., Faraday Trans. II* **1979**, 880.

(15) Hara, A.; Gondo, Y. *J. Chem. Phys.* **1986**, *85*, 1894.

(16) Lin, Y.; Nelson, M. C.; Hanson, D. M. *J. Chem. Phys.* **1987**, *86*, 1586.

(17) Ito, S.; Katayama, H.; Yamamoto, M. *Macromolecules* **1988**, *21*, 2456.

(18) Nagai, K.; Takamiya, N.; Kaneko, M. *J. Photochem. Photobiol. A: Chem.* **1994**, *84*, 271.

(19) See, for example: Dorfman, R. C.; Tachiya, M.; Fayer, M. D. *Chem. Phys. Lett.* **1991**, *179*, 152. (b) Dorfman, R. C.; Lin, Y.; Fayer, M. D. *J. Phys. Chem.* **1989**, *93*, 6388. (c) Lin, Y.; Dorfman, R. C.; Fayer, M. D. *J. Chem. Phys.* **1989**, *90*, 159. (d) Dominque, R. P.; Fayer, M. D. *J. Chem. Phys.* **1985**, *83*, 2242.

(20) Yamamoto, K.; Takemura, T.; Baba, H. *J. Lumin.* **1977**, *15*, 445.

(21) Rothe, C.; King, S.; Monkman, A. *Nat. Mater.* **2006**, *5*, 463.

(22) (a) Merkel, P. B.; Dinnocenzo, J. P. *J. Photochem. Photobiol. A: Chem.* **2008**, *193*, 110. (b) Cavaleri, J. J.; Prater, K.; Bowman, R. M. *Chem. Phys. Lett.* **1996**, *259*, 495.

(23) Perrin, F. *Comp. Rend.* **1924**, *178*, 1978.

(24) Dexter, D. L. *J. Chem. Phys.* **1953**, *21*, 836.

(25) Huddleston, R. K.; Miller, J. R. *J. Phys. Chem.* **1982**, *86*, 200.

(26) (a) Hertz, P. *Math. Ann.* **1909**, *67*, 387. (b) Chandrasekhar, S. *Rev. Mod. Phys.* **1943**, *15*, 1. see p 86.

(27) You, Z.-Q.; Hsu, C.-P.; Fleming, G. R. J. *Chem. Phys.* **2006**, *124*, 044506.

(28) Molecular volumes were calculated with Spartan'04 (ver. 1.0.3, Wavefunction, Inc.).

(29) In solution exothermic triplet energy transfer is usually nearly diffusion limited and in most cases does not tend to show an "inverted" behavior at high exothermicities. This may reflect the accommodation of large exothermicities by energy transfer to higher triplet states of A. Exothermic energy transfer involving highly distorted triplets may be less than diffusion limited in solution and give rise to lower k_0 values in rigid media.

(30) Pilling, M. J.; Seakins, P. W. *Reaction Kinetics*; Oxford University Press: Oxford, 1995; pp 146−156.

(31) Alternatively, a value for k_{-d} may be calculated from the Eigen expression (Eigen, M. *Z. Phys. Chem.* **1954**, *1*, 176.), according to which $k_{-d} = 3000k_d/4\pi(r_{D+A})^3N$. With $k_d = 1.5 \times 10^{10}$ M^{-1} s^{-1} and $r_{D+A} = 6.5$ Å, we obtain $k_{-d} = 2.2 \times 10^{10}$ s^{-1}, similar to the value estimated from K_{DA}.

(32) Anderson, R. W.; Hochstrasser, R. M.; Lutz, H.; Scott, G. W. *J. Chem. Phys.* **1974**, *61*, 2500.

(33) Rikenglaz, M. M.; Rozman, I. M. *Opt. Spectosc.* **1974**, *36*, 61.

(34) On the basis of the density of 0.90 and our calculated van der Waals volume of 111 $Å^3$ a free volume of about 32% at 295° C may be estimated for ethyl acetate. At 77 K ethyl acetate undergoes a shrinkage of about 20%, reflecting a loss in free volume.

(35) Ferry, J. D. *Viscoelastic Properties of Polymers*; John Wiley & Sons, Inc: New York, 1980. See Table 11-II.

(36) Guerry-Butty, E.; Haselbach, E.; Suppan, P. *Chimia* **1994**, *48*, 391.

(37) (a) Kirkwood, J. G. *J. Chem. Phys.* **1939**, *7*, 919. (b) McQuarrie, D. A. *Statistical Mechanics*; Haper and Row: New York, 1976. See Figure 13-3.

(38) Waring, J. R.; Lovell, R.; Mitchell, G. R.; Windle, A. H. *J. Mater. Sci.* **1982**, *17*, 1171.

(39) Blumen, A. *J. Chem. Phys.* **1980**, *72*, 2632.

(40) Morgan, J. R.; El Sayed, M. A. *J. Phys. Chem.* **1983**, *87*, 2178.

(41) For highly-allowed singlet−singlet coulombic energy transfer from 1-chloroanthracene (1CA) to perylene (P) the half-quenching distance at which the energy-transfer rate constant, k_{et}, equals the radiative rate constant of 1CA of $\sim 10^8$ s^{-1} is ~40 Å (Turro, N. J. Modern Molecular Photochemistry; University Science Books, Sausalito, CA, 1991; pp 322−324). Assuming the extent of overlap of D emission and A absorption remains nearly constant k_{et} varies as the radiative rate, k_D, of the excited donor × the extinction coefficient, ϵ_A, of the A transition and inversely as the sixth power of the separation distance, r (Turro, N. J. Modern Molecular Photochemistry; University Science Books, Sausalito, CA, 1991; p 303.). For ^{3}PXAN, k_D is only about $10^{-7} \times k_D$ for 1CA, and for the S_0-T_1 transition of TPDC, ϵ_A is about 10^{-8} as large as ϵ_A for P. This yields a k_{et} of only about 0.03 s^{-1} for coulombic energy transfer from ^{3}PXAN to TPDC at 10 Å, the closest noncontact D/A separation allowed by the molecules of the medium.

(42) In both solution and rigid media k_0 represents an orientation-averaged value. Research of Fayer and co-workers[19d] indicates that electron-transfer kinetics in rigid media appears to be functionally independent of orientation, i.e., angle averaged, at times > 1 ns.

(43) Experiments of Gray, Winkler, and coworkers indicated that rates of long-range electron transfer depend upon the medium.[44] To the extent that this also applies to electron exchange, the k_0 appropriate for ^{3}D and A in contact may not be appropriate when they are separated by molecules of the medium.

(44) (a) Wenger, O. S.; Gray, H. B.; Winkler, J. R. *Chimia* **2005**, *59*, 94. (b) Wenger, O. S.; Leigh, B. S.; Villahermosa, R. M.; Gray, H. B.; Winkler, J. R. *Science* **2005**, *307*, 99.

(45) Kobashai, H.; Morita, T.; Mataga, N. *Chem. Phys. Lett.* **1973**, *20*, 376.

JP802164D